

Fast Fourier Transform computations and build-up of plastic deformation in 2D, elastic-perfectly plastic, pixelwise disordered porous media

F. Willot^{1,2}, Y.-P. Pellegrini¹

¹ Département de Physique Théorique et Appliquée, CEA, BP12, 91680 Bruyères-le-Châtel, France

² Laboratoire de Mécanique des Solides, École Polytechnique, 91128 Palaiseau, France

francois.willot@lms.polytechnique.fr, yves-patrick.pellegrini@cea.fr

ABSTRACT: Stress and strain fields in a two-dimensional pixelwise disordered system are computed by a Fast Fourier Transform method. The system, a model for a ductile damaged medium, consists of an elastic-perfectly matrix containing void pixels. Its behavior is investigated under equibiaxial or shear loading. We monitor the evolution with loading of plastically deformed zones, and we exhibit a nucleation / growth / coalescence scenario of the latter. Identification of plastic “clusters” is eased by using a discrete Green function implementing equilibrium and continuity at the level of one pixel. Observed morphological regimes are put into correspondence with some features of the macroscopic stress / strain curves.

Keywords: Plasticity, ductile damage, FFT, localization, disorder.

1 INTRODUCTION

The versatile Fast Fourier Transform (FFT) method of Moulinec, Suquet, and Michel represented a breakthrough in the computation of the stress and strain fields in linear or nonlinear composites. This method uses the Lippmann-Schwinger integral equation of the strain field in a homogeneous reference linear medium, written in the Fourier space. Nonlinearity is embedded via a pointwise heterogeneous polarization field which depends on the constitutive law, and which is computed in direct space. The integral equation is solved iteratively through FFT and inverse FFT transformations for which efficient routines are available. The ill-convergence of the basic iterative procedure is alleviated by use of an “augmented Lagrangian method” and by Uzawa’s algorithm, see [1] for details.

With some modifications, this method is used hereafter to investigate the build-up and incipient localization of plastic deformation in elastic-perfectly plastic porous pixelwise disordered systems [2]. Such systems consist of an on-lattice realization of a random system where the material properties of adjacent material elements are statistically uncorrelated from point to point, in the limit where the size of the material element goes to zero. Other realizations of this type of disorder (in the bond form) include random spring or resistor networks. Such systems are particularly attractive as benchmarks for homogenization methods, since their microscopic disorder correlation length is the smallest possible. Then, the self-consistent linear effective medium approximation is exact to fourth order in correlations (in the sense of diagram expansions, e.g. [3]), as has been shown for dielectric media or for random resistors networks (RRNs) [3].

2 DISCRETE GREEN FUNCTION IN FFT CALCULATIONS

A two-dimensional (2D) square lattice of pixels (i, j) of size L^2 is considered. Pixels are either randomly chosen as voids, in concentration f , or as elastic-perfectly plastic

matter elements with flow stress Y . Deformation theory [4] is used. Using the continuum Green tensor of the strain (GT) as in [1] (we call this approach ‘‘CG1’’), we observe that : (i) convergence of the FFT method is slow for infinite contrast; (ii) the fields, and the plastically deformed zone where the Mises norm of the stress σ_{eq} is locally equal to the flow stress Y exhibit a spurious ‘‘checkerboard’’ pattern (see Fig. 1) which complicates a subsequent identification of plastic clusters (cf. Sec. 3).

Discrete Green functions — In the alternative solution considered here, introducing the unit vectors along the axes $\hat{\mathbf{e}}^i$ such that $e_j^i = \delta_{ij}$ (the Kronecker symbol), we follow the RRN scheme of Ref. [3] and use forward and backward finite-difference schemes for the compatibility and equilibrium equations (discrete Fourier Transforms in elasticity are also used in Ref. [5]):

$$\varepsilon_{ij}(\mathbf{x}) = \frac{1}{2} [u_j(\mathbf{x} + \hat{\mathbf{e}}^i) - u_j(\mathbf{x}) + (i \leftrightarrow j)], \quad \sum_j [\sigma_{ij}(\mathbf{x}) - \sigma_{ij}(\mathbf{x} - \hat{\mathbf{e}}^j)] = 0. \quad (1)$$

Contrary to a centered-difference scheme, equilibrium is enforced here on any finite connex subset of pixels. In the discrete Fourier representation with discrete Fourier momenta $q_i = 2\pi m_i/L$, $m_i = 0, 1, \dots, L-1$ (the conventions of Ref. [3] are used), these equations read [here $i = (-1)^{1/2}$]:

$$\varepsilon_{kl} = (i/2) (k_k u_l + k_l u_k), \quad ik_l^* \sigma_{kl} = 0, \quad \text{with} \quad k_j \equiv 2 \sin(q_j/2) e^{iq_j/2}, \quad (2)$$

where $*$ denotes the complex conjugate. The associated GT for the strain is:

$$G_{ijkl}(\mathbf{q}) = - \left(N_{jl}^{-1} k_i k_k^* + N_{il}^{-1} k_j k_k^* + N_{jk}^{-1} k_i k_l^* + N_{ik}^{-1} k_j k_l^* \right) / 4 \quad (3)$$

where the acoustic tensor is $N_{ij} \equiv k_k^* C_{ijkl} k_l$ with C_{ijkl} the elastic tensor of the isotropic reference medium of Lamé moduli μ and λ . The restriction to generalized plane strain loading (fields independent of z) is obtained by setting $q_3 = 0$ and retaining only the indices $i, j, k, l = 1, 2$. Though an analytic expression of G is available [2], the inversion of \mathbf{N} is most easily carried out numerically. The continuum GT (e.g. [1]) is retrieved in the long wavelength limit $q_1, q_2 \ll 1$. A centered-difference scheme would instead lead to a real GT, simply obtainable from the continuum GT by replacing its Fourier momenta by $k_j \equiv \sin(q_j)$.

The GT (3) does not comply with the square symmetry of the grid, and lacks major symmetry, due to its nonzero imaginary part: $G_{ijkl} = G_{klji}^*$. The inconsistency comes from the fact that the equilibrium equation in (1) is a balance condition for forces transmitted by *bonds* linking nearest-neighbor pixels, whereas the constitutive law used is appropriate for material points only, i.e. the pixels. As a result, the forward and backward directions on a each cartesian axis are not equivalent, which leads to asymmetric field patterns. Two easy work-arounds are considered. The first one, called *discrete Green 1* (DG1), consists in replacing (3) by its symmetrized version

$$G_{ijkl}^{(1)} \equiv \{ G_{ijkl}(q_1, q_2) + G_{ijkl}(-q_1, -q_2) + (-1)^{i+j+k+l} [G_{ijkl}(-q_1, q_2) + G_{ijkl}(q_1, -q_2)] \} / 4. \quad (4)$$

This GT corresponds to no discretization scheme in direct space, but should be interpreted as the GT of some non-local medium in which the stiffness tensor C_{ijkl} is replaced by a non-local convolution kernel with finite range of order 1. The second way, called DG2, consists in carrying out four different calculations on the same system up to final convergence, employing each one of the four $G_{ijkl}(q_1, q_2)$, $G_{ijkl}(-q_1, -q_2)$, $G_{ijkl}(-q_1, q_2)$, $G_{ijkl}(q_1, -q_2)$ in turn, and in taking the average of the four converged

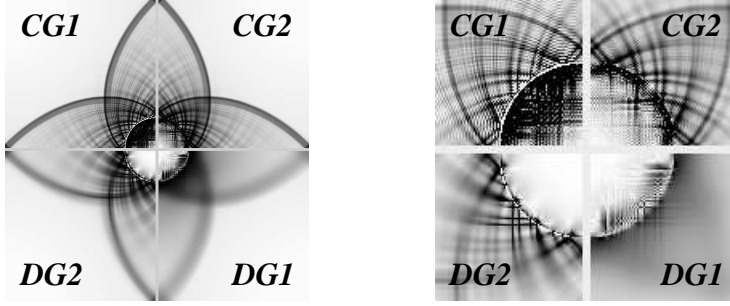


Figure 1: Differences between the methods. Periodic case with one void under equibiaxial loading. The gray field shows the equivalent strain field norm, $\varepsilon_{\text{eq}} = [(2/3)\varepsilon'_{ij}\varepsilon'_{ij}]^{1/2}$, where $\varepsilon'_{ij} = \varepsilon_{ij} - \delta_{ij}\varepsilon_{kk}/3$. Pixels near the void surface with the highest field values have been thresholded out ($\sim 1.5\%$ of the total number). The right image is an enlargement.

strain fields as the final result. We also consider, for comparison purposes, field pictures obtained from CG1 by means of a local average post-processing consisting in taking 5-point averages on the current pixel and its four nearest neighbors. We call this the CG2 method.

Setting $k^2 = k_1^2 + k_2^2$, the 2D displacement field is obtained from $\varepsilon_{ij}(\mathbf{q})$ using (the mode $q = 0$ is irrelevant):

$$u_1(\mathbf{q}) = -\frac{i}{k^2} \{k_1 [\varepsilon_{11} - \varepsilon_{22}] + 2k_2 \varepsilon_{12}\}, \quad u_2(\mathbf{q}) = \frac{i}{k^2} \{k_2 [\varepsilon_{11} - \varepsilon_{22}] - 2k_1 \varepsilon_{12}\}.$$

In the computations hereafter, the bulk and shear moduli are $K = 1$ and $\mu = 0.4$ and $Y = 0.5$. The loading is prescribed by imposing an overall strain, which is increased until the stress reaches its flow value [1].

Differences between the methods are illustrated in Fig. 1, where the equivalent shear strain in a periodic medium under equi-biaxial loading is displayed, in quadrants of a unit cell with one circular void (volume fraction $f = 0.1$).¹ Method CG2 does not suppress the “checkerboard” pattern of method CG1. Method DG1 blurs excessively the strain field. The best result without “checkerboard” effect is obtained with DG2. The strain field inside the void depends on the method, but is physically irrelevant.

Convergence issues — Two convergence indicators are used. First, we require the stress divergence (computed in Fourier representation) to be such that $\langle \|\text{div}\boldsymbol{\sigma}\|^2 \rangle < \eta_1^2 \langle \boldsymbol{\sigma} \rangle : \langle \boldsymbol{\sigma} \rangle$. Additional steps of the iterative algorithm are then carried out until $\langle \boldsymbol{\sigma}^{n+1} - \boldsymbol{\sigma}^n \rangle : \langle \boldsymbol{\sigma}^{n+1} - \boldsymbol{\sigma}^n \rangle < \eta_2^2 \langle \boldsymbol{\sigma}^{n+1} \rangle : \langle \boldsymbol{\sigma}^{n+1} \rangle$ between steps n and $n + 1$. The overall prescribed tolerance is specified by the pair (η_1, η_2) . For benchmarking, typical values of $\eta_{1,2}$ of order 10^{-5} , and system sizes $L = 512, 1024, 2048$ were considered. For both the periodic void lattice and the pixelwise disordered medium on which we focus hereafter, method DG2 converges faster (i.e., in fewer iterations) than CG1. The absolute precision on the average stress, extrapolated to infinite system sizes by an inverse power law fit of the size dependence, is then typically 10^{-3} . For

¹The strain localization motif, of a surprisingly rich sub-structure – remark the bands of finite width which bound the localization zone – is approximately made of logarithmic spirals leaving the void surface at angle 45° [4] as predicted by slip-line theory (e.g., [4]), though the lines are somehow distorted and blurred by lattice effects.

more precise calculations, values of $\eta_{1,2}$ of order 10^{-8} and system size $L = 4096$ have been used (see [2] for details).

3 BUILD-UP OF PLASTIC DEFORMATION IN THE POROUS MEDIUM

Using method DG2, we investigate the link between the overall stress-strain curve and the development of the plastic zones where $\sigma_{\text{eq}} = Y$ in a pixelwise disordered porous medium. The medium can be considered as made of three phases: elastic (where $\sigma_{\text{eq}} < Y$), porous (where $\sigma = 0$), and plastic ($\sigma_{\text{eq}} = Y$). Under increasing loading, plastic zones develop starting from the voids (around which the shear stress is larger), grow, coalesce and eventually “percolate” in the system. Void or plastic clusters, are identified (with the Hoshen-Kopelman algorithm [6]) as pixel sets of same phase connected by the nearest-neighbour criterion. The “void-plastic” phase comprises the voids and the plastic zones. In this phase the local tangent shear modulus is zero. Due to local unloading effects (possibly an artefact of the – reversible – deformation theory), purely plastic clusters in the vicinity of the pores can temporarily disconnect during the first loading stages, especially under shear loading. This has bearing on cluster counting. This was corrected by modifying the first-neighbor connectivity rule: we furthermore connect to the nearest void, each plastic cluster not already connected to a void. Each cluster then contains one void at least.

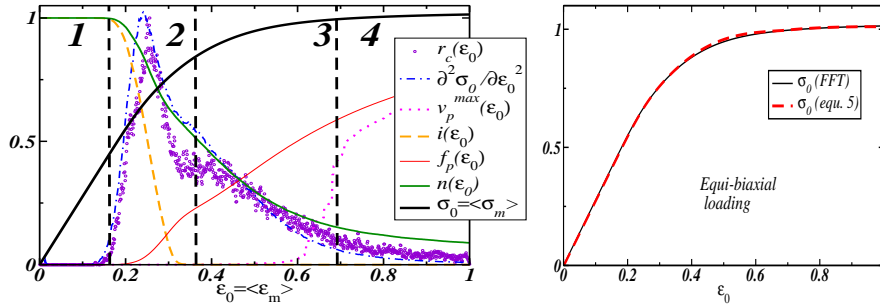


Figure 2: Equi-biaxial loading. Left: stress-strain curve and geometric indicators as a function of the applied overall strain. Right: empirical stress-loading formula compared to FFT stress/strain curve.

Equi-biaxial loading — Fig. 2 (left) displays, for a porosity $f = 0.01$, various geometrical indicators, as a function of the applied equi-biaxial overall strain $\varepsilon_0 = \langle \varepsilon_m \rangle$, along with the macroscopic equibiaxial stress/strain curve $\sigma_0 = \langle \sigma_m \rangle(\varepsilon_0)$ (the brackets denote a spatial average), and the opposite of its second derivative $-\partial^2 \sigma_0 / \partial \varepsilon_0^2$: the normalized volume fraction of void-plastic zone $f_p = v_p / (1 - f)$ where v_p is the volume fraction of void-plastic zone; the volume fraction v_{max} of the largest void-plastic cluster; the proportion of isolated voids clusters $i(\varepsilon_0)$ (i.e. voids not connected to a plastic zone); the number $n(\varepsilon_0)$ of void-plastic clusters (normalized to the number of voids at $\varepsilon_0 = 0$); and the coalescence rate $r(\varepsilon_0) = \partial n(\varepsilon_0) / \partial \varepsilon_0$, multiplied by a magnifying factor so as to make it conspicuous on the curve. Four characteristic regimes are isolated, marked on the figure: (1) elastic loading regime: the number of isolated voids remains constant; (2) growth of plastic zones around the voids: the number of isolated voids diminishes, f_p grows approximately quadratically, the coalescence rate develops a huge peak (coalescence between plastic clusters originating from neighboring voids). The regime ends up as $i(\varepsilon_0) = 0$, all voids having developed a plastic zone; (3) regime of stabilized coalescence: f_p increases linearly, the coalescence rate somewhat stabilizes, then decreases more slowly as a largest void-

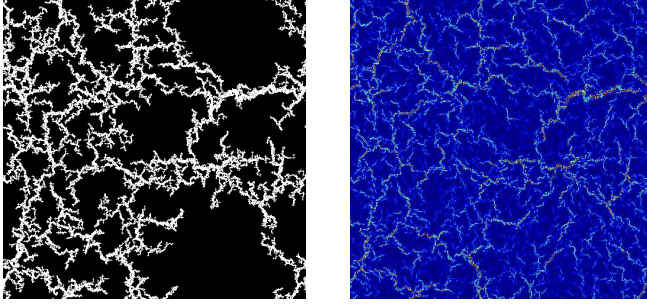


Figure 3: Equi-biaxial loading for porosity $f = 0.1$. Left: largest void-plastic cluster (white) at percolation ($\varepsilon_0 \simeq 0.9$). Right: equivalent norm of the shear strain field at a larger overall strain ($\varepsilon_0 = 1.1$).

plastic cluster emerges; (4) stress saturation regime: it begins at the percolation of the void-plastic zone where the largest plastic cluster grows fast, and where f_p increases slower than linearly with the strain. From these observations, we see that the second derivative of the stress-strain curve is strongly correlated to the coalescence rate, and that the macroscopic flow stress attains its final order of magnitude at percolation of the plastic zone through the medium. Typical plastic clusters and shear strain field are displayed in Fig. 3. Their fractal character will be discussed elsewhere. The shear strain is strongly localized (but not uniform) within the plastic zones.

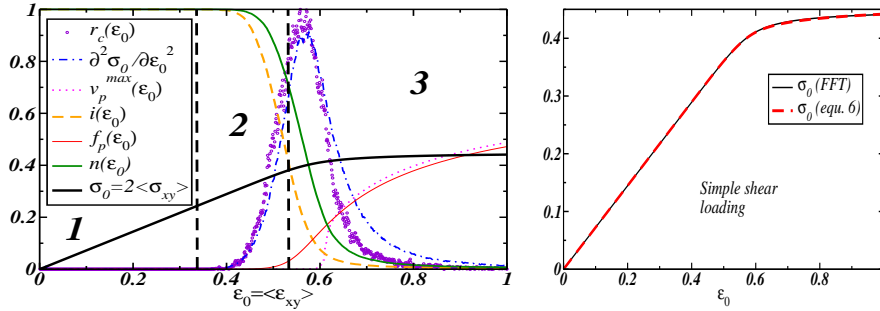


Figure 4: Simple shear loading. Same legend as fig. 2.

Loading in simple shear — Fig. 4 (left) displays the same quantities as Fig. 2, for the same medium, in simple shear loading where $\varepsilon_0 = \langle \varepsilon_{xy} \rangle$ and $\sigma_0 = \langle \sigma_{xy} \rangle$. The main difference is the disappearance of the stabilized coalescence regime. Fig. 5 displays a typical instance of the fields for a weak porosity, with straight shear bands.

Empirical formula for the stress-strain curve — Amusingly, one can reproduce the stress-strain curves using the above geometric indicators and the porosity-dependent effective compressibility and shear elastic moduli \tilde{K} and $\tilde{\mu}$. We indeed arrived at the empirical formulae (the effective elastic moduli are computed on the simulated system):

$$\sigma_0 \simeq \tilde{K}(f) \int_0^{\varepsilon_0} d\varepsilon_0 \left\{ \frac{n(\varepsilon_0) - n(\infty)}{1 - n(\infty)} + \alpha [v_p(\varepsilon_0) - v_p^{\max}(\varepsilon_0)] \right\}, \quad (5)$$

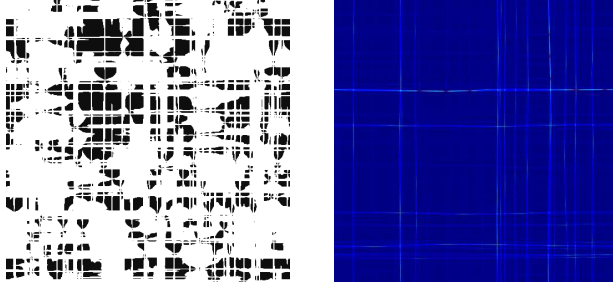


Figure 5: Simple shear loading at $f = 10^{-4}$. System size $L = 1024$ at applied strain $\varepsilon_0 = 2$. Left: plastic (white) and elastic (black) zones. Right: equivalent norm of the shear strain field.

$$\sigma_0 \simeq \alpha f_p + 2\tilde{\mu}(f) \int_0^{\varepsilon_0} d\varepsilon_0 \frac{n(\varepsilon_0) - n(\infty)}{1 - n(\infty)}, \quad (6)$$

where (5) and (6) apply to pressure and shear loadings respectively, and where α is a fitting number different in each case. In both expressions, the term containing cluster numbers reproduces the zone of maximal curvature of the stress-strain curve (regime of maximal coalescence rate), whereas the plastic volume fraction enters the description of the saturation regime. These formulae are compared to the FFT stress / strain curves in Figs. 2 and 3 (right). Though the present “guesswork” should not be taken too seriously (in particular, the dependence of α with respect to f has not been studied, and the plastic volume fraction does not enter both formulas in the same manner), such an approach might nonetheless ultimately contribute to enrich the effective-medium approach to porous media. Indeed taking correlations into account so as to incorporate microstructural information in the effective-medium framework is a notoriously difficult problem. The possibility of using global indicators of geometric nature such as the fraction of plastic zone, or cluster numbers, for which phenomenological evolution models could be proposed might then constitute a useful alternative.

Acknowledgments: Y.-P.P. thanks Pierre Suquet for drawing his attention to Ref. [5].

References

- [1] J.-C. Michel, H. Moulinec and P. Suquet. A computational method based on augmented Lagrangians and Fast Fourier Transforms for composites with high contrast. *Comput. Model. Eng. Sci.*, 1:79–88, 2000, and references therein.
- [2] F. Willot. *Contribution à l’étude théorique de la localisation plastique dans les poreux*. PhD. thesis, École Polytechnique, 2007 (in French). <http://www.imprimerie.polytechnique.fr/Theses/Files/Willot.pdf>.
- [3] J.-M. Luck. Conductivity of random networks: an investigation of the accuracy of the effective-medium approximation. *Phys. Rev. B*, 43:3933–3944, 1991.
- [4] J. Lubliner. *Plasticity theory*. Macmillan, New York, 1990.
- [5] W. Dreyer, W.H. Müller, J. Olchewski. An approximate analytical 2D-solution for the stresses and strains in eigenstrained cubic materials. *Acta Mech.*, 136: 171–192, 1999.
- [6] D. Stauffer, A. Aharony. *An introduction to percolation theory*. Taylor and Francis, London, 1985.